

We are IntechOpen, the world's leading publisher of Open Access books Built by scientists, for scientists

6,900

Open access books available

186,000

International authors and editors

200M

Downloads

Our authors are among the

154

Countries delivered to

TOP 1%

most cited scientists

12.2%

Contributors from top 500 universities



WEB OF SCIENCE™

Selection of our books indexed in the Book Citation Index
in Web of Science™ Core Collection (BKCI)

Interested in publishing with us?
Contact book.department@intechopen.com

Numbers displayed above are based on latest data collected.
For more information visit www.intechopen.com



Micro-Inertial-Aided High-Precision Positioning Method for Small-Diameter PIG Navigation

Lianwu Guan, Xu Xu, Yanbin Gao, Fanming Liu,
Hanxiao Rong, Meng Wang and
Aboelmagd Noureldin

Additional information is available at the end of the chapter

<http://dx.doi.org/10.5772/intechopen.80343>

Abstract

Pipeline leakage or explosion has caused huge economic losses, polluted the environments and threatened the safety of civilian's lives and assets, which even caused negative influences to the society greatly. Fortunately, pipeline inspection gauge (PIG) could accomplish the pipeline defect (corrosions, cracks, grooves, etc.) inspection effectively and meanwhile to localize these defects precisely by navigation sensors. The results are utilized for pipeline integrity management (PIM) and pipeline geographic information system construction. Generally, the urban underground pipeline presents with small-diameter and complicated-distribution properties, which are of great challenges for the pipeline defects positioning by PIG. This chapter focuses on in-depth research of the high-precision positioning method for small-diameter PIG navigation. In the beginning, the problems and system errors statement of MEMS SINS-based PIG are analyzed step by step. Then, the pipeline junction (PJ) identification method based on fast orthogonal search (FOS) is studied. After that, a PIG positioning system that comprises of micro-inertial/AGM/odometer/PJ is proposed, and also the application mechanism of extended Kalman filter and its smoothing technology on PIG navigation system is researched to improve the overall positioning precision for the small-diameter PIG. Finally, the proposed methods and research conclusions are verified by the indoor wheel robot simulation platform.

Keywords: micro-inertial navigation, small-diameter PIG, pipeline junction, fast orthogonal search, extended Kalman filter and smoothing technology

1. Introduction

Pipeline is one of the useful transportation tools to deliver the gases or liquids from the starting point to the different user destinations effectively and safely. For example, in Canada, 97% of the raw oil and gas production is transported by pipeline according to the Canadian energy pipelines association (CEPA) data [1]. Moreover, the total length of routed pipelines used for oil and gas transportation has exceeded 600,000 km in North America [2]. However, when pipeline is operated over its designed life expectancy, and also when meets with natural disasters or human damages, the pipeline is easily broken and causes the leakage of gas or oil [3]. The leakage would lead to the environmental pollution, explosion, even lives in danger especially when the leakage or explosion occurred in urban areas with high populations. Therefore, the detection as well as positioning of pipeline defects by pipeline inspection gauge (PIG) is of great importance to fulfill the pipeline integrity management (PIM) and pipeline geographic information system (GIS) construction.

Generally, the pipeline detection methods include in-pipeline inspection and outer-pipeline inspection. But depending on the requirements of transportation and the land-usage reasons, almost most of the pipeline is buried underground. That is to say, it is extremely difficult, time-consuming, and expensive to reach and inspect the pipeline from its outside. Therefore, PIG is designed to inspect the existed or potential pipeline defects in the inner or outer surface of pipeline by driven with the gas or liquid in the pipeline, which could improve the safety rate of operational pipeline to be 99.99% under related regulations [4]. In addition, PIG is usually equipped with various electronic devices to record the physical data about the pipeline situation and to analyze them offline.

Pipeline defect inspection and localization are two main missions for a PIG system [5]. Magnetic flux leakage (MFL) and ultrasonic (UT) are the main inspection technologies that is usually used to detect the pipeline defects when installing in the PIG [6]. The information provided by these technologies need to be synchronized with the positioning technology to obtain pipeline defect coordinates accurately for PIM and GIS construction. Generally, inertial navigation system (INS) is to be more suitable for this purpose than GPS because the satellite signal from GPS is completely interrupted by the Earth and the steel-structured pipeline. Moreover, the 3D orthogonal accelerations and 3D orthogonal angular rates of PIG are measured by inertial measurement unit (IMU), and these measurements are adopted to determine the coordinates of pipeline centerline by INS mechanization [7]. Meanwhile, the horizontal and vertical pipeline curvatures could also be calculated to expose the potential pipeline bend or displacement [8]. A typical PIG that carries the inspection sensors with strapdown INS (SINS) is shown in **Figure 1**.

Different from the navigation in other applications, the motions of PIG inside the inspected pipeline are comprised of its longitudinal rotation motion (rolling) and the regular traveling motion along the pipeline longitudinal direction [9]. The PIG rolling motion could improve its go-through capability in some wax obstacle or heavy sludge areas at the bottom part of the pipeline. Meanwhile, the inspection capability for the pipeline inspection sensors on potential pipeline defects is improved significantly by PIG rolling motion. Furthermore, the rolling motion enhances the positioning precision of SINS-based PIG navigation, and therefore improves the

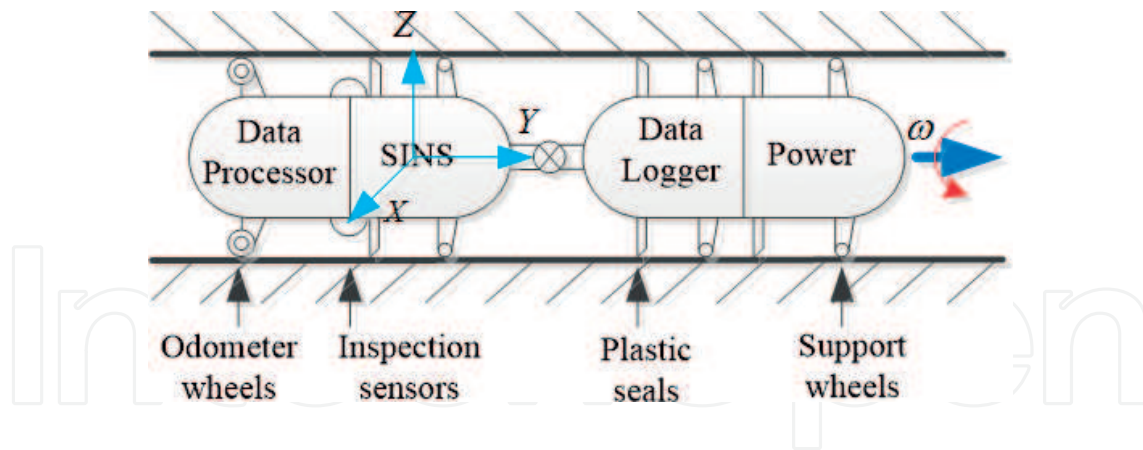


Figure 1. A typical PIG for inner-pipeline inspection.

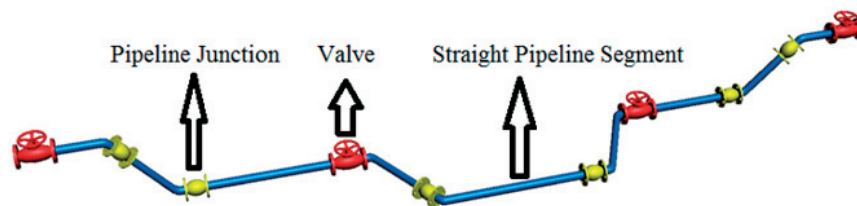


Figure 2. A typical pipeline with PJs and valves.

pipeline defect positioning precision that minimizes the costs and labor involved for PIM and GIS building for the inspected pipeline.

A normal pipeline is demonstrated in **Figure 2**; the pipeline junction (PJ) is usually used to connect the two adjacent straight pipeline segments (SPSs) and also connect the pipeline to the valve. The azimuth and pitch angles of the PIG in each SPS are constant because the cylinder-shaped PIG is constrained by pipeline in the horizontal and vertical directions [10]. Hence, the detection of the PJs could provide azimuth and pitch angle updates and improve the positioning precision for SINS-based PIG.

This chapter aims to have an in-depth research of its high-precision positioning method for the small-diameter PIG navigation. At the beginning, the unique movement characteristic of PIG is analyzed in Section 2. Then, the PJ detection method based on fast orthogonal search (FOS) is studied to implement the PJ detection accurately in Section 3. After that, a PIG positioning system that comprises of micro-inertial/AGM/odometer/PJ is proposed and also the application mechanism of extended Kalman filter (EKF) and its smoothing technology on the PIG positioning system is researched to improve the overall positioning precision for the small-diameter PIG in Section 4. The proposed methods and research experiments are performed in Section 5. Finally, the conclusions are summarized in Section 6.

2. The MEMS SINS-based PIG

Currently, most of the PIG navigation system is comprised of fiber optic gyroscope (FOG)-based SINS when the diameter of pipeline is over 12." However, due to the volume constrain,

the FOG SINS cannot be used in the small-diameter pipeline-based PIG. Fortunately, with the rapid development of microelectromechanical-system (MEMS) technology, the positioning precision of MEMS SINS improved greatly and it accelerates the application of MEMS SINS in small-diameter PIG. Therefore, considering the cost, size, weight, and power consumption, the small-volume MEMS SINS is superior for pipeline defects localization when its diameter is less than 12" [11]. However, the pipeline defects positioning error of MEMS SINS is divergent with the distance enlargement of the inspected pipeline. The main reason is the error of MEMS inertial sensors is much greater than that of the usually used FOG inertial sensors-based pipeline navigation application [12].

2.1. The problem statement of MEMS SINS-based PIG

At present, the rear part of PIG is symmetrically installed with odometers to measure its longitudinal velocity and meanwhile reduce the slippage-induced velocity error, which is used for the reduction of the time-accumulated error of SINS in PIG. Meanwhile, zero-velocity updates in both lateral and vertical directions of cylinder-shaped PIG are provided by its nonholonomic constraint (NHC) characteristic. Hence, there are 3D continuous velocity updates for SINS of PIG. Moreover, the 3D coordinates of pipeline valves and above-ground markers (AGMs) are provided by DGPS, which are used for 3D sporadic coordinate updates for SINS of PIG [13]. Nevertheless, the continuous 3D velocity and sporadic 3D coordinate updates cannot satisfy the surveying precision requirements in small-volume MEMS SINS-based pipeline navigation system in small diameter pipeline.

Apart from the velocity and position errors, the attitude error (pitch error δp , roll error δr , and azimuth error δA) also degrades the positioning precision of MEMS SINS-based PIG. The change rates of PIG horizontal velocity errors $\delta \dot{v}_n$ and $\delta \dot{v}_e$ are given by [14]:

$$\begin{cases} \delta \dot{v}_n = -f_u \delta p + f_e \delta A + \delta f_n \\ \delta \dot{v}_e = -f_u \delta r + f_n \delta A + \delta f_e \end{cases} \quad (1)$$

where, δf_e and δf_n denote accelerometer biases in Earth east and north directions. f_e , f_n , and f_u denote acceleration components in Earth east, north, and up directions.

In Eq. (1), the value of f_u is close to local Earth gravity and it is much bigger than f_e and f_n in PIG navigation application. Hence, the pitch and roll errors of SINS in PIG are tightly coupled with the corresponding horizontal velocity errors, and the 3D velocity errors of PIG are observable by odometers and NHC. Therefore, the azimuth error of SINS in PIG is not observable, while the pitch and roll errors are observable. The horizontal position errors of SINS in PIG are obtained by twice integration on the change rate of azimuth-error-induced horizontal velocity errors [14]:

$$\begin{cases} \delta \dot{v}_{n2} = f_e \delta A \\ \delta \dot{v}_{e2} = -f_n \delta A \end{cases} \rightarrow \begin{cases} \delta P_{n2}(t_k) = \delta P_{n2}(t_{k-1}) + v_e \delta A \Delta t \\ \delta P_{e2}(t_k) = \delta P_{e2}(t_{k-1}) - v_n \delta A \Delta t \end{cases} \quad (2)$$

where $\Delta\delta P_{n2}$ and $\Delta\delta P_{e2}$ are the azimuth-error-induced horizontal position errors. They are also related to PIG horizontal velocities v_e and v_n , and the time interval Δt . More intuitively, when PIG travels with 1 m/s in horizontal velocity, and 1° in azimuth error, the position error that caused by azimuth error is about 89 m in 1 h of PIG navigation. Therefore, to correct the azimuth error is an important way to enhance the navigation precision of SINS-based PIG.

At present, azimuth sensors, like camera, magnetometer, and optical navigation sensor are usually adopted to improve the measurement precision of azimuth, but both the cost and weight of PIG would increase. Moreover, their measurement precision is also severely degraded by the pipeline application [8]. So, it is not viable for these sensors to be applied to correct the azimuth error of PIG accurately. However, it is worth noting that the routed pipeline is connected by fixed-length SPS via PJ. The cylinder-shaped PIG makes the azimuth and pitch maintain constant from the beginning to the end of each SPS. Therefore, the azimuth and pitch mechanized by SINS at the beginning of SPS are usually used as updates in the corresponding SPS. Consequently, the PJ detection result provides azimuth and pitch updates for MEMS SINS, and the PJ detection would be analyzed in Section 3.

2.2. The system error model of MEMS SINS-based PIG

For the SINS-based PIG navigation system, the system error model is given by [14]:

$$\delta\dot{x} = \begin{bmatrix} F_{11} & F_{12} & 0_{3*3} & 0_{3*3} & 0_{3*3} \\ F_{21} & F_{22} & F_{23} & 0_{3*3} & R_b^n \\ F_{31} & F_{32} & F_{33} & R_b^n & 0_{3*3} \\ 0_{3*3} & 0_{3*3} & 0_{3*3} & F_{44} & 0_{3*3} \\ 0_{3*3} & 0_{3*3} & 0_{3*3} & 0_{3*3} & F_{55} \end{bmatrix} \delta x + Gw \quad (3)$$

where

$$F_{11} = \begin{bmatrix} 0 & 0 & -\dot{\phi}/(R_M + h) \\ \dot{\lambda} \tan \phi & 0 & -\dot{\lambda}/(R_N + h) \\ 0 & 0 & 0 \end{bmatrix}, F_{23} = \begin{bmatrix} 0 & f_u & -f_n \\ -f_u & 0 & f_e \\ f_n & -f_e & 0 \end{bmatrix},$$

$$F_{12} = \begin{bmatrix} 0 & \frac{1}{R_M + h} & 0 \\ \frac{1}{(R_N + h) \cos \phi} & 0 & 0 \\ 0 & 0 & 1 \end{bmatrix}, F_{32} = \begin{bmatrix} 0 & \frac{1}{R_M + h} & 0 \\ \frac{-1}{R_N + h} & 0 & 0 \\ \frac{-\tan \phi}{R_N + h} & 0 & 0 \end{bmatrix},$$

$$F_{21} = \begin{bmatrix} 2\omega_e(v_u \sin \phi + v_n \cos \phi) + \dot{\lambda}v_n/\cos \phi & 0 & 0 \\ -2\omega_e v_e \cos \phi - \dot{\lambda}v_e/\cos \phi & 0 & 0 \\ -2\omega_e v_e \sin \phi & 0 & 2g/R_N \end{bmatrix},$$

$$\begin{aligned}
F_{22} &= \begin{bmatrix} (v_n \tan \phi - v_u)/(R_N + h) & (2\omega_e + \dot{\lambda}) \sin \phi & -(2\omega_e + \dot{\lambda}) \cos \phi \\ -2(\omega_e + \dot{\lambda}) \sin \phi & -v_u/(R_M + h) & -\dot{\phi} \\ 2(\omega_e + \dot{\lambda}) \cos \phi & 2\dot{\phi} & 0 \end{bmatrix}, \\
F_{31} &= \begin{bmatrix} 0 & 0 & -\dot{\lambda}/(R_M + h) \\ \omega_e \sin \phi & 0 & \dot{\lambda} \cos \phi/(R_N + h) \\ -\omega_e \cos \phi - \dot{\lambda}/(R_N + h) \cos \phi & 0 & \dot{\lambda} \sin \phi/(R_N + h) \end{bmatrix}, F_{44} = \begin{bmatrix} -\beta_{\omega x} & 0 & 0 \\ 0 & -\beta_{\omega y} & 0 \\ 0 & 0 & -\beta_{\omega z} \end{bmatrix}, \\
F_{33} &= \begin{bmatrix} 0 & (\omega_e + \dot{\lambda}) \sin \phi & -(\omega_e + \dot{\lambda}) \cos \phi \\ -(\omega_e + \dot{\lambda}) \sin \phi & 0 & -\dot{\phi} \\ (\omega_e + \dot{\lambda}) \cos \phi & \dot{\phi} & 0 \end{bmatrix}, F_{55} = \begin{bmatrix} -\beta_{f_x} & 0 & 0 \\ 0 & -\beta_{f_y} & 0 \\ 0 & 0 & -\beta_{f_z} \end{bmatrix}
\end{aligned}$$

and, ϕ and λ are local latitude and longitude, $\dot{\phi} = v_n/(R_M + h)$, $\dot{\lambda} = v_e/(R_M + h) \cos \phi$. R_M , R_N , and h are meridian radius, normal radius, and geodetic height. The system state variables are $\delta x = [\delta r^n \ \delta v^n \ \varepsilon^n \ \delta \omega^n \ \delta f^n]^T$. R_b^n is the transformation matrix from body frame to navigation frame. And w is system noise, the system noise matrix is expressed [14] as

$$G = \begin{bmatrix} O_{9 \times 1}, \sqrt{2\beta_{\omega x} \sigma_{\omega x}^2}, \sqrt{2\beta_{\omega y} \sigma_{\omega y}^2}, \sqrt{2\beta_{\omega z} \sigma_{\omega z}^2}, \sqrt{2\beta_{f_x} \sigma_{f_x}^2}, \sqrt{2\beta_{f_y} \sigma_{f_y}^2}, \sqrt{2\beta_{f_z} \sigma_{f_z}^2} \end{bmatrix}^T \quad (4)$$

where $\beta_{\omega x}$, $\beta_{\omega y}$ and $\beta_{\omega z}$ are the reciprocals of the correlation times of autocorrelation sequence of $\delta \omega_x$, $\delta \omega_y$ and $\delta \omega_z$; $\sigma_{\omega x}$, $\sigma_{\omega y}$ and $\sigma_{\omega z}$ are variance associated with gyroscope errors. β_{f_x} , β_{f_y} and β_{f_z} are the reciprocals of the correlation times of autocorrelation sequence of δf_x , δf_y and δf_z ; σ_{f_x} , σ_{f_y} and σ_{f_z} are variance associated with accelerometer errors.

3. PJ identification by fast orthogonal search

In **Figure 2**, the azimuth and pitch of PIG are invariant when it travels inside the SPS; they only changed at the PJ part. In addition, the roll of PIG is varied with the PIG rolling motion in the pipeline [15]. Therefore, the precise identification of the PJs between two adjacent SPSs could provide accurate azimuth and pitch updates indication for SINS in the corresponding SPS.

This section introduces a novel PJ detection technique by using FOS to analyze the MEMS accelerometer data. FOS is a random method that is used for the short-term signal processing, the time series analysis, and the complex system identification [16]. The simulated data sets are acquired when IMU is installed on the triaxial positioning and rate table at first. Then, the accelerometer data are analyzed and extracted by wavelet and FOS, respectively. After that, the detection result reveals the FOS could detect PJ from accelerometer data sets successfully when it is compared with the wavelet. Finally, FOS-based PJ detection result could provide indication for the azimuth and pitch updates in the corresponding SPS [16].

3.1. FOS-based PJ detection

3.1.1. Fast orthogonal search

FOS has been adopted in denoising and random error modeling of MEMS inertial sensors successfully [17]. An arbitrary set of nonorthogonal candidate function $p_m(n)$ is used to discover a functional expansion of an input $y(n)$ by minimizing the mean squared error (MSE) between $p_m(n)$ and $y(n)$ [18]. The input $y(n)$ in terms of the $p_m(n)$ is presented:

$$y(n) = \sum_{m=0}^M a_m p_m(n) + \varepsilon(n) \quad (5)$$

where $a_m (m = 1, 2, \dots, M)$ are the weights of $p_m(n)$, and $\varepsilon(n)$ is the model error.

The principle of FOS is to rediscover the right side of Eq. (5) into a sum of terms that are mutually orthogonal from $n = 0$ to N of the overall portion of the data:

$$y(n) = \sum_{m=0}^M g_m w_m(n) + e(n) \quad (6)$$

where $w_m(n) (m = 1, 2, \dots, M)$ denote the orthogonal functions that are generated from $p_m(n)$ by Gram-Schmidt orthogonalization method, which are yield by

$$w_m(n) = p_m(n) - \sum_{r=0}^{m-1} \alpha_{mr} w_r(n) \quad (7)$$

where

$$\alpha_{mr} = \frac{\sum_{n=0}^N p_m(n) w_r(n)}{\sum_{n=0}^N (w_r(n))^2} \quad (8)$$

$$g_m = \frac{\sum_{n=0}^N y(n) w_m(n)}{\sum_{n=0}^N (w_m(n))^2} \quad (9)$$

The orthogonal expansion coefficients g_m are calculated to achieve a least-squares fitting:

$$MSE = \sum_{n=0}^N \left(y_n - \sum_{m=0}^M g_m w_m(n) \right)^2 / (N + 1) \quad (10)$$

However, the construction of orthogonal expansion function $w_m(n)$ in Eq. (7) is high time and memory consumption. Here, the FOS computes the orthogonal expansion coefficients g_m without explicitly creating the orthogonal function $w_m(n)$ to significantly reduce the computing time and memory requirements consequently. The coefficients g_m are calculated by

$$g_m = C(m)/D(m, m), m = 0, \dots, M \quad (11)$$

where

$$D(m, 0) = 1, D(m, m) = \overline{p_m(n)}, D(m, r) = \overline{p_m(n)p_r(n)} - \sum_{i=0}^{r-1} \alpha_{mi}(m, i) \quad (12)$$

$$\alpha_{mr} = D(m, r)/D(r, r), m = 1, \dots, M; r = 1, \dots, m$$

with

$$C(0) = \overline{y(n)}; C(m) = \overline{y(n)p_m(n)} - \sum_{r=0}^{m-1} \alpha_{mr}C(r) \quad (13)$$

The MSE in Eq. (10) is equivalent to

$$MSE = \overline{y^2(n)} - \sum_{m=0}^M g_m^2 D(m, m) \quad (14)$$

The overbar of the previous equations is the time average that calculated over the portion of data recorded from $n = 0$ to N .

The MSE reduction given by math model addition is

$$Q_m = g_m^2 \overline{w_m^2(n)} = g_m^2 D(m, m) \quad (15)$$

Therefore, FOS could search a model with a few fitting terms that reduce the MSE in order of its significance. Generally, FOS is terminated by one of the following three conditions. The first is when the predefined number of terms reached. The second is when the ratio of MSE to the mean squared value of the input signal is under a preset threshold. The third is when the reduction of the MSE by adding another term to the model is less than fitting the white Gaussian noise (WGN). FOS is completed by selecting the candidates $p_m(n)$ that are the pairs of sine and cosine functions at the interested frequencies. The candidate functions $p_m(n)$ are

$$\begin{cases} p_{2m-1}(n) = \sin(\omega_m n) \\ p_{2m}(n) = \cos(\omega_m n) \end{cases} \quad (16)$$

where $\omega_m(m = 1, 2, \dots, K)$ and K are the digital frequency and the number of the candidate frequency, respectively.

3.1.2. Design of FOS for PJ detection

In PJ detection, the accelerometer measurement data are transformed to a different domain by FOS to model the PIG motion dynamics from the inertial sensor measurement, and meanwhile to reject as much of the noises of inertial sensor as possible. In addition, the FOS extracts the

singularity signals from the inertial sensors by its amplitude when maintaining the PJ detection precision.

The length of data record, the candidate functions, and the termination conditions could be used to determine the modeling accuracy of the FOS. The long-time recorded data are usually divided into a few short segments [19], and the each segment is modeled by FOS to extract the dynamic components from the noisy measurements. Furthermore, the frequency, amplitude, and phase of recorded data are included in the output of each segment of the FOS model terms, which could be utilized to synthesize an estimation of the true motion dynamics. Finally, all the segments are repeated by this process separately and recombined to implement the overall modeled data.

3.2. PJ detection implemented by FOS

3.2.1. Experimental equipment

Low-cost MEMS IMU Crossbow IMU300CC could measure the PIG triaxial angular rates and linear accelerations. Moreover, the Ideal Aerosmith 2103HT positioning and rate table are used to simulate the pipeline trajectory as shown in **Figure 2**. The experimental equipment of Crossbow IMU300CC, 2103HT table, table control panel, inertial sensors data acquisition system, and their corresponding connection are shown in **Figure 3**.

3.2.2. Experimental procedures

The simulated pipeline trajectory is similar to the one shown in **Figure 2**. The outer, middle, and inner table rotation axes are operated to accomplish the PIG attitude angles changes. Specifically, the rotation of table inner axis indicates that when PIG runs in the pipeline, it would experience varying degrees of rolling motion. The table middle axis could simulate the changes of pitch, and

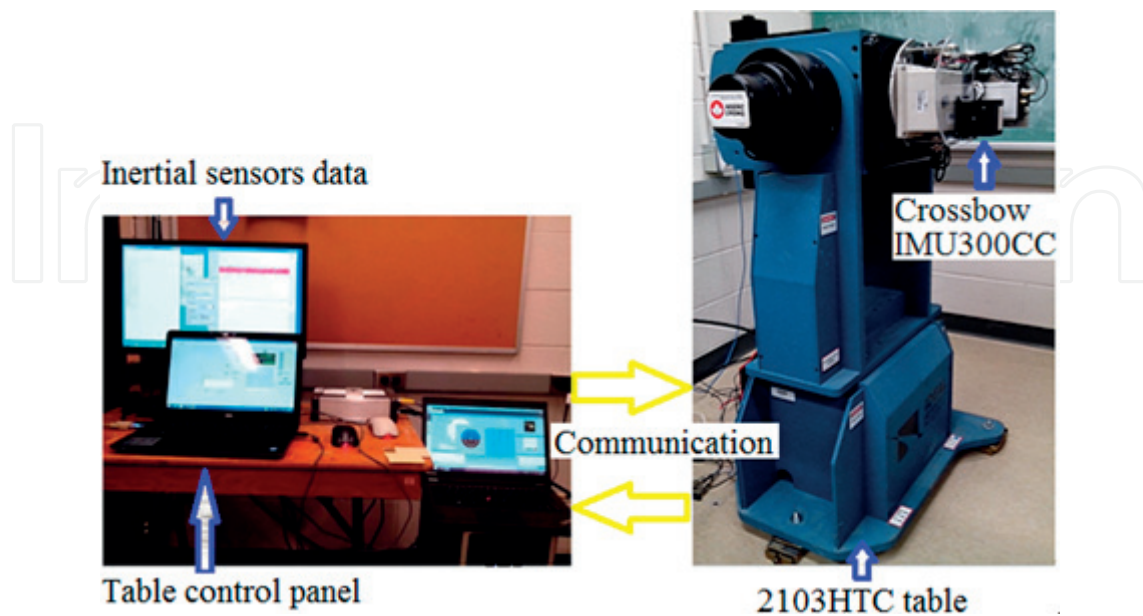


Figure 3. Crossbow IMU300CC and 2103HT table.

the PIG azimuth angle variations are simulated by table outer axis. The experiment is designed by as the following:

Firstly, the table rotates around the middle axis for 90° to make the PIG in horizontal plane as shown in right panel of **Figure 3**, which simulates the PIG launcher stage for pipeline inspection, and keeps this position for a few minutes to complete the initial alignment.

Secondly, the table middle axis rotates from horizontal position to -45° , which simulates the PIG movement from launcher to the underground pipeline.

Thirdly, the table middle axis rotates back to horizontal plane to simulate the starting of the regular PIG navigation stage.

Thirdly, rotate the outer axis every once in a while, to simulate the PIG runs in different pipeline segments with different azimuth angles.

Fourthly, move the table middle axis to 45° , which simulates the PIG movement from pipeline to receiver, then the middle axis rotates back to keep the PIG horizontal.

Finally, save and download the measurement data of inertial sensors, and the overall experiment period cost about 1700s.

3.2.3. Experimental result and discussion

Due to the rolling motion of PIG, the X-axis accelerometer in IMU is used for the data analysis, which is shown in **Figure 4**. The blue curve shows the raw X-axis accelerometer measurement

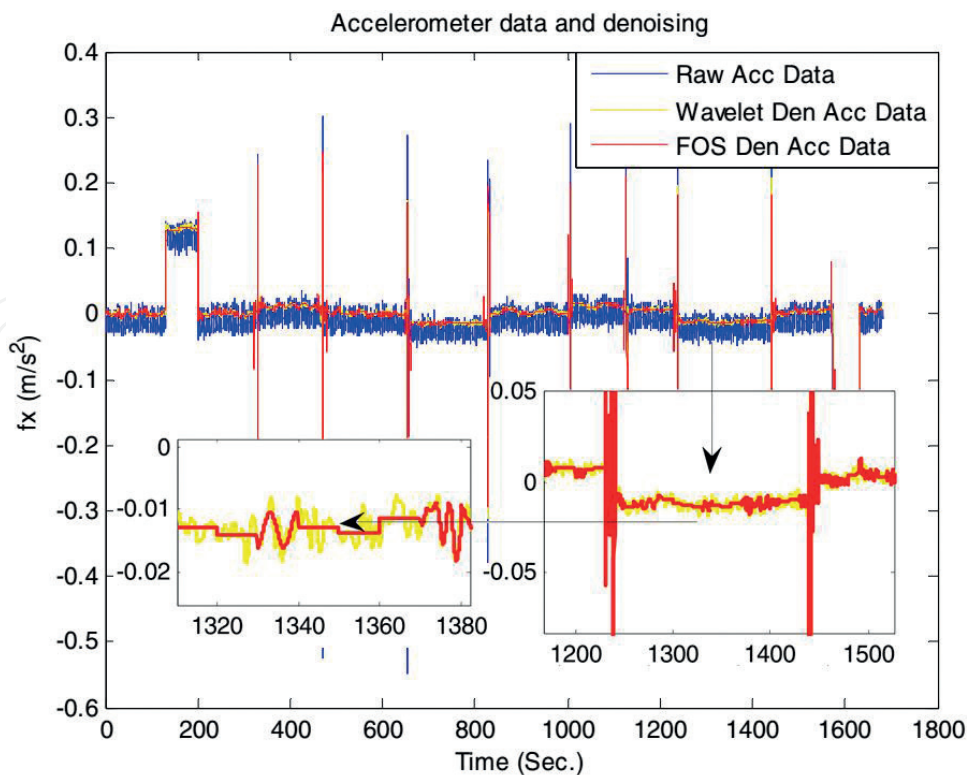


Figure 4. Raw accelerometer data (blue curve), wavelet denoised data (yellow curve), and FOS denoised data (red curve).

data that is contaminated by high Gaussian white noise (GWN). Hence, it is necessary to conduct data denoising before the PJ detection. The “db” family of wavelet was certificated to be a useful selection for the denoising of MEMS inertial sensors data [19]. Here, “db8” wavelet with four level of decomposition (LOD) is used for denoising on the accelerometer measurement data, and the result is demonstrated by yellow curve in **Figure 4**. In addition, FOS has shown superior performance in the denoising of low-cost MEMS inertial sensors in some applications [20], and the FOS denoised accelerometer data are represented by red curve in **Figure 4**. Both methods could provide robust MEMS accelerometer data denoising by reducing the random GWN level and maintaining the dynamic characteristic of the PIG. Moreover, FOS has shown significant improvement in the elimination of low-frequency noises, which could not be eliminated by wavelet denoising technology. Therefore, FOS is more suitable for low-cost MEMS inertial sensors for PJ detection application.

The upper panel in **Figure 5** reveals the raw measurement data of X-axis accelerometer. The jumps or spikes are the singular signals that expected to be identified accurately to provide azimuth and pitch updates in SPS. The lower panel of **Figure 5** also displays the amplitude that is calculated by FOS after the raw measurement data of accelerometer are denoised by FOS. The amplitude and the epochs indicate the singular signals of the raw measurement data of accelerometer.

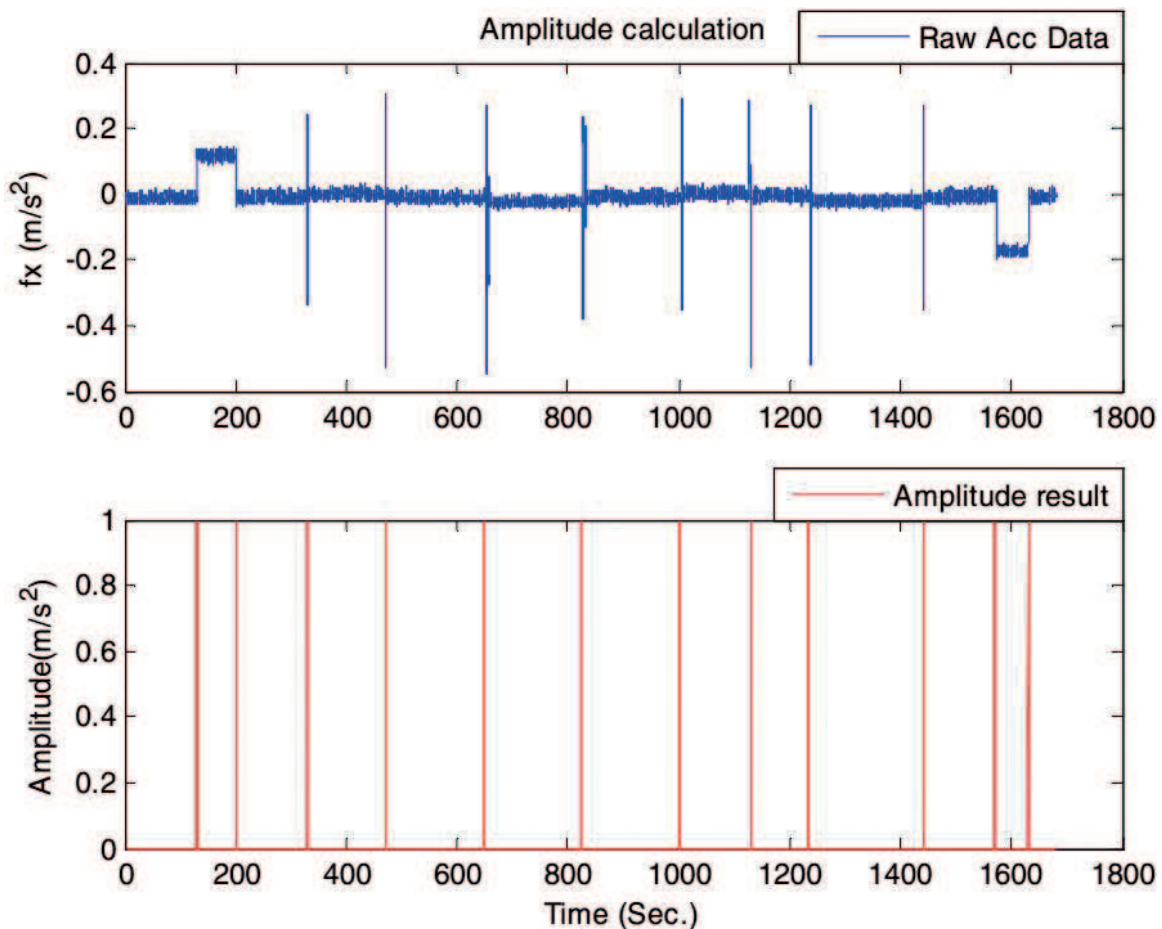


Figure 5. Raw X-axis accelerometer data (upper panel) and FOS amplitude (lower panel).

Figure 6 displays the PJ identification result by FOS on denoised measurement data of X-axis accelerometer. Specifically, the PJG passing through a PJ part is represented by the spike intervals in the red curve. These spikes are calculated by the preset threshold on the FOS amplitude. That is to say, when the FOS amplitude is bigger than the threshold, the intervals are detected as the PJs, while the other intervals are detected as SPSs. Furthermore, a magnified view of the second and third PJs in the **Figure 6** is also demonstrated to make the PJ detection result to be more intuitive. Specifically, a pitch angle variation of the PJG is shown by the second PJ, while an azimuth angle variation of the PJG is revealed by the third PJ. Therefore, the PJ could be detected correctly by FOS even with the raw accelerometer data in GWN-contaminated environment. After that, the accurate PJ detection results can be used for azimuth and pitch updates at the SPS in SINS.

The **Figures 4–6** shows the FOS-based PJ detection method on accelerometer measurement data for PJG navigation. The accelerometer measurement data are logged by using 2103HT table to simulate the azimuth and pitch changes of PJG in the pipeline. Moreover, the detection capability and precision of FOS are also verified with the FOS technology on accelerometer measurement data. The final results demonstrated that the FOS could detect the PJ correctly even when the accelerometer data contaminated with high GWN. Therefore, the proposed FOS can detect the PJ by measurement of the low-cost inertial sensors even in noised pipeline operational environments.

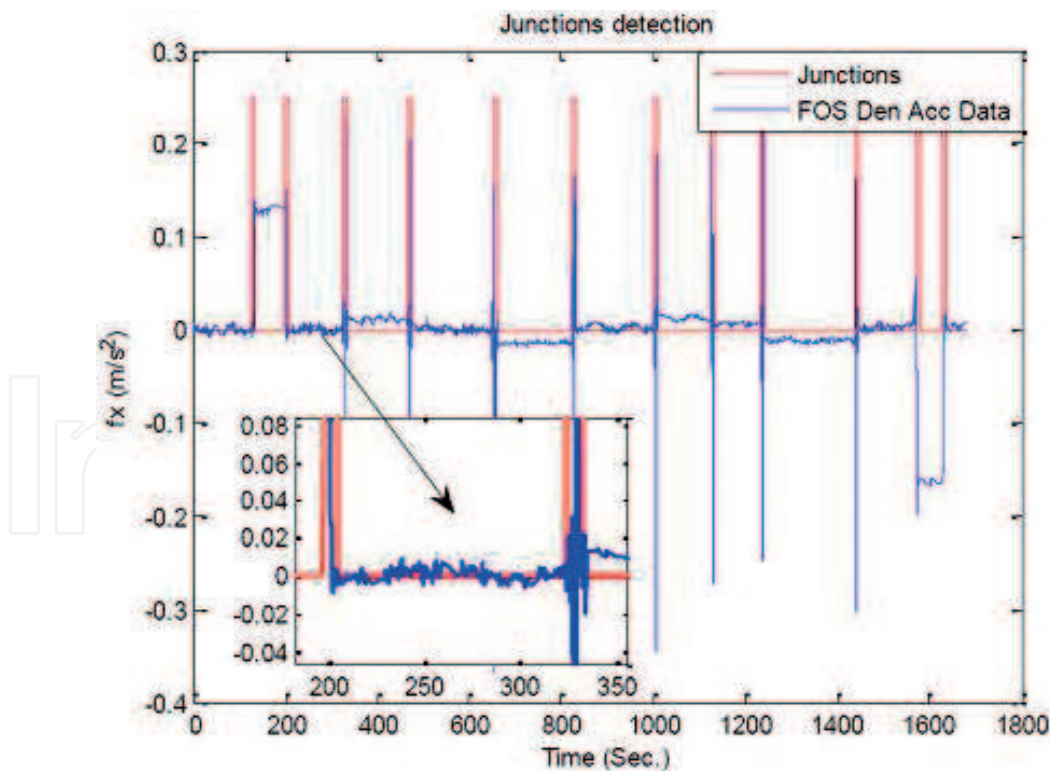


Figure 6. PJ recognition result by FOS.

4. MEMS SINS-enhanced PIG navigation system by PJ detection in small-diameter pipeline

In the above sections, the constant azimuth and pitch angles could be used to estimate the SINS errors in SPS. Therefore, this section would introduce an MEMS SINS-enhanced pipeline navigation system by PJ detection.

4.1. Introduction of micro-inertial/AGM/odometer/PJ system

Figure 7 shows the schematic diagram of the micro-inertial/AGM/odometer/PJ pipeline navigation system. The triaxial angular rate ω and triaxial linear acceleration f of PIG are measured by micro-inertial sensors in the pipeline. Then, the 3D attitude, velocity, and position of the PIG are provided by SINS mechanization. In order to correct the micro-inertial-sensor-error-induced PIG navigation error, the overall measurement updates include:

- continuous azimuth and pitch updates in each SPS that are provided by PJ detection result,
- 3D continuous velocity updates provided by odometers and PIG NHCs in pipeline, and
- 3D sporadic coordinate updates provided by DGPS in the AGMs for every few kilometers.

Furthermore, these updates are both integrated by EKF and Rauch-Tung-Striebel smoother (RTSS) to estimate and correct the errors of micro-inertial sensors and the PIG navigation system [21].

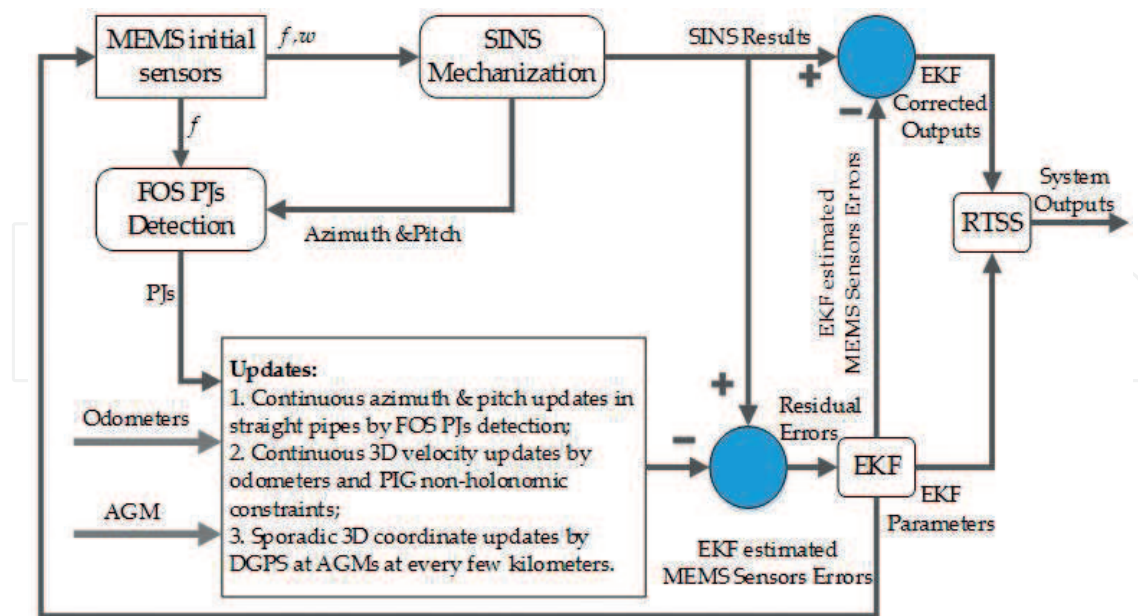


Figure 7. Schematic of micro-inertial/AGM/odometer/PJ-based pipeline navigation system.

4.2. Measurement models of micro-inertial/AGM/odometer/PJ system

The system error model is provided in Section 2.2. For the measurement state variables, there are four kinds of measurement models when PIG staying in different stages of the pipeline [22].

Firstly, when there are no AGMs in SPS, the measurement model of micro-inertial/odometer/PJ system is given by:

$$\begin{bmatrix} v_{e,m} - v_{e,SINS} \\ v_{n,m} - v_{n,SINS} \\ v_{u,m} - v_{u,SINS} \\ p_{PJ} - p_{SINS} \\ A_{PJ} - A_{SINS} \end{bmatrix} = H_1 \delta x - \begin{bmatrix} \delta \eta_{ve} \\ \delta \eta_{vn} \\ \delta \eta_{vu} \\ \delta \eta_p \\ \delta \eta_A \end{bmatrix} \quad (17)$$

where $v_{e,m}$, $v_{n,m}$ and $v_{u,m}$ are the 3D velocity measurement updates from odometers and PIG NHCs. $v_{e,SINS}$, $v_{n,SINS}$ and $v_{u,SINS}$ are the 3D velocity calculated by SINS. $\delta \eta_{ve}$, $\delta \eta_{vn}$ and $\delta \eta_{vu}$ are the velocity measurement noise. p_{PJ} and A_{PJ} denote the pitch and azimuth angles that are calculated by SINS at the beginning of each SPS, respectively; $\delta \eta_p$ and $\delta \eta_A$ are the corresponding measurement noises. Therefore, the system measurement matrix H_1 is

$$H_1 = \begin{bmatrix} O_{3*3} & I_{3*3} & O_{3*3} & O_{3*6} \\ O_{2*3} & O_{2*3} & H_{1,1} & O_{2*6} \end{bmatrix}, H_{1,1} = \begin{bmatrix} 1 & 0 & 0 \\ 0 & 0 & 1 \end{bmatrix}$$

Secondly, when there are AGMs in SPS, the system measurement model of micro-inertial/AGM/odometer/PJ is expressed as:

$$\begin{bmatrix} \varphi_{AGM} - \varphi_{SINS} \\ \lambda_{AGM} - \lambda_{SINS} \\ h_{AGM} - h_{SINS} \\ v_{e,m} - v_{e,SINS} \\ v_{n,m} - v_{n,SINS} \\ v_{u,m} - v_{u,SINS} \\ p_{PJ} - p_{SINS} \\ A_{PJ} - A_{SINS} \end{bmatrix} = H_2 \delta x - \begin{bmatrix} \delta \eta_\varphi \\ \delta \eta_\lambda \\ \delta \eta_h \\ \delta \eta_{ve} \\ \delta \eta_{vn} \\ \delta \eta_{vu} \\ \delta \eta_p \\ \delta \eta_A \end{bmatrix} \quad (18)$$

where φ_{SINS} , λ_{SINS} , and h_{SINS} are the PIG position calculated by SINS mechanization. φ_{AGM} , λ_{AGM} , and h_{AGM} are the AGM position provided by DGPS. $\delta \eta_\varphi$, $\delta \eta_\lambda$, and $\delta \eta_h$ denote the AGM position measurement noise. Hence, the system measurement matrix H_2 is:

$$H_2 = \begin{bmatrix} I_{6*6} & O_{6*3} & O_{6*6} \\ O_{2*6} & H_{2,1} & O_{2*6} \end{bmatrix}, \text{ and } H_{2,1} = \begin{bmatrix} 1 & 0 & 0 \\ 0 & 0 & 1 \end{bmatrix}.$$

Thirdly, when there are no AGMs in PJ part, the system measurement model of micro-inertial/odometer is expressed as:

$$\begin{bmatrix} v_{e,m} - v_{e,SINS} \\ v_{n,m} - v_{n,SINS} \\ v_{u,m} - v_{u,SINS} \end{bmatrix} = H_3 \delta x - \begin{bmatrix} \delta \eta_{ve} \\ \delta \eta_{vn} \\ \delta \eta_{vu} \end{bmatrix} \quad (19)$$

and the system measurement matrix H_3 is:

$$H_3 = [O_{3*3} \quad I_{3*3} \quad O_{3*9}].$$

Fourthly, when there are AGMs in the PJ part, the system measurement model of micro-inertial/AGM/odometer is

$$\begin{bmatrix} \varphi_{AGM} - \varphi_{SINS} \\ \lambda_{AGM} - \lambda_{SINS} \\ h_{AGM} - h_{SINS} \\ v_{e,m} - v_{e,SINS} \\ v_{n,m} - v_{n,SINS} \\ v_{u,m} - v_{u,SINS} \end{bmatrix} = H_4 \delta x - \begin{bmatrix} \delta \eta_{\varphi} \\ \delta \eta_{\lambda} \\ \delta \eta_h \\ \delta \eta_{ve} \\ \delta \eta_{vn} \\ \delta \eta_{vu} \end{bmatrix} \quad (20)$$

The system measurement matrix H_4 is

$$H_4 = [I_{6*6} \quad O_{6*9}]$$

During the measurement update stage of micro-inertial/AGM/odometer/PJ-based pipeline navigation system, the odometers and NHCs of PIG provide 3D continuous velocity updates, AGMs provide 3D sporadic coordinate updates, and PJ detection provides continuous azimuth and pitch updates in SPS. Therefore, when obtaining the EKF gain K_{Fk} , system states updates $\delta \hat{x}_{Fk}^+$ and system states covariance matrix P_{Fk}^+ ; the system design matrix H_k and the measurement covariance matrix R_k are calculated by the system measurement updates z_k when PIG in SPS or PJ part.

5. Experiments and results analysis

5.1. Experimental equipment

Husky A200™ robot (Figure 8 left panel) from Clearpath Robotics of Canada is adopted to simulate the near-real situation of PIG running in an inspected pipeline. The pipeline-navigation-related sensors include VTI IMU, odometer, and so on. Specifically, two odometers are used in the left and right rear wheels of the robot for reducing the velocity measurement

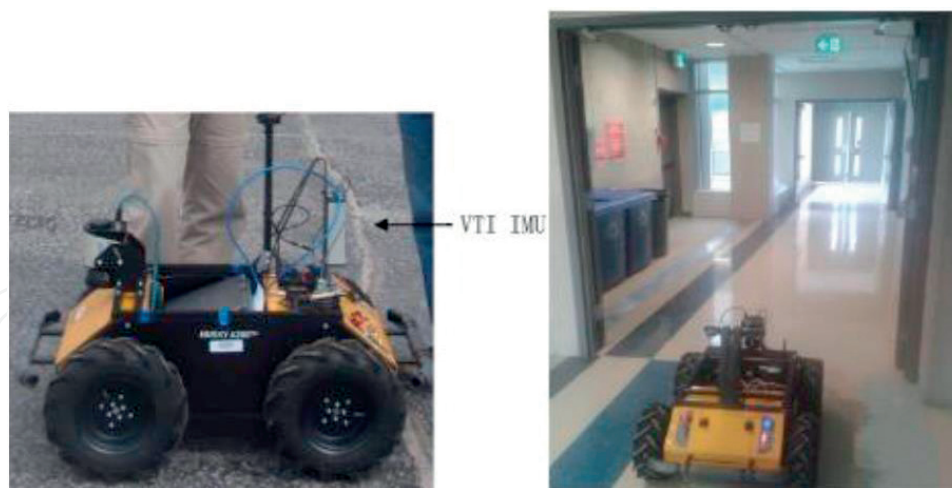


Figure 8. Husky A200™ robot and the experiment corridor.

error of micro-inertial sensors. In addition, the movement of this robot in straight line at the straight corridor can be controlled with remote controller, and the ground in the experiments is roughly horizontal (**Figure 8** right panel), which are adopted to simulate the NHCs and to eliminate the slippage of wheels of the FIG.

5.2. Experiment procedures

In the simulation experiment, Husky A200™ robot moves in a near rectangle corridor, which is around 70 m in length and 40 m in width. The detailed control parameters of Husky A200™ robot are set as following:

- a. The forward velocity of the Husky A200™ robot is near 1 m/s, and it moves in a fixed direction in each straight corridor, which simulates the FIG running in straight pipeline.
- b. The robot turns 90° at the end point of each straight corridor and, meanwhile, to keep the robot running, which is used to simulate the FIG go through the bend pipeline.
- c. In each long and straight corridor, the protrusion is preset at every 5–10 m to simulate the movement of FIG over the circular weld or the flange.
- d. The overall length of the experiment in each closed circle is about 220 m, and only the coordinates of start point and final point are used as coordinate updates.

In addition, the whole experiment is conducted within indoor and seven landmarks are derived from the coordinates measured by DGPS from roof corners of the experimental building to be set as referenced landmarks.

Figure 9 displays seven red landmarks at some corners of the rectangular corridor, which are derived by the seven yellow circle coordinates at the roof corners of the experimental building. Moreover, the starting point or final point of the experiment is shown on the upper right position of the floor map by a star symbol.

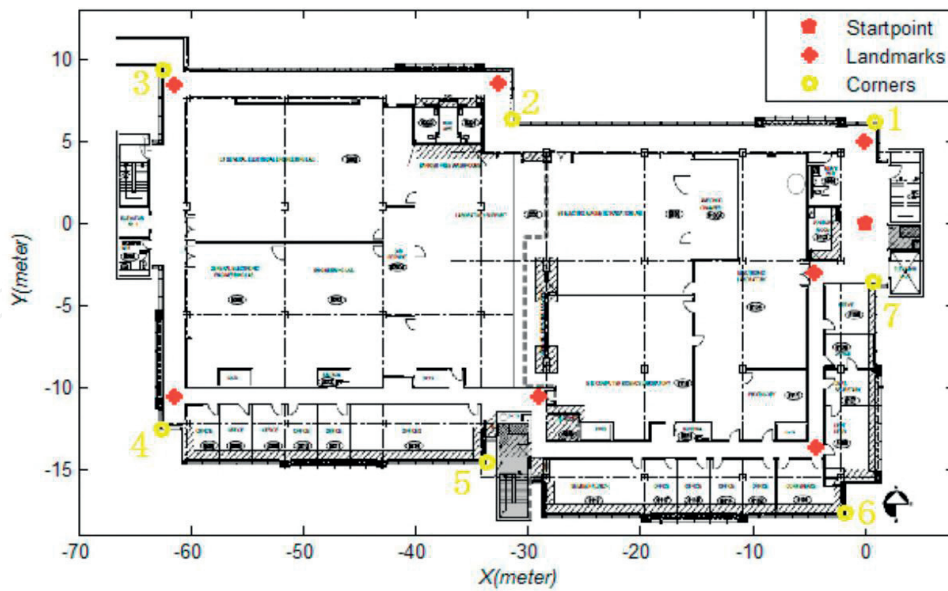


Figure 9. The landmarks for the experiment in corridor.

5.3. Experimental results and analysis

5.3.1. Pipeline junction detection

In **Figure 10**, the PJ detection result is obtained by Z-axis accelerometer measurement data of VTI IMU with FOS. The blue and red signals denote the raw and denoised accelerometer measurement data, respectively. The difference between the blue and red signals not only revealed the feasibility of FOS denoising on VTI IMU, but also demonstrated that the

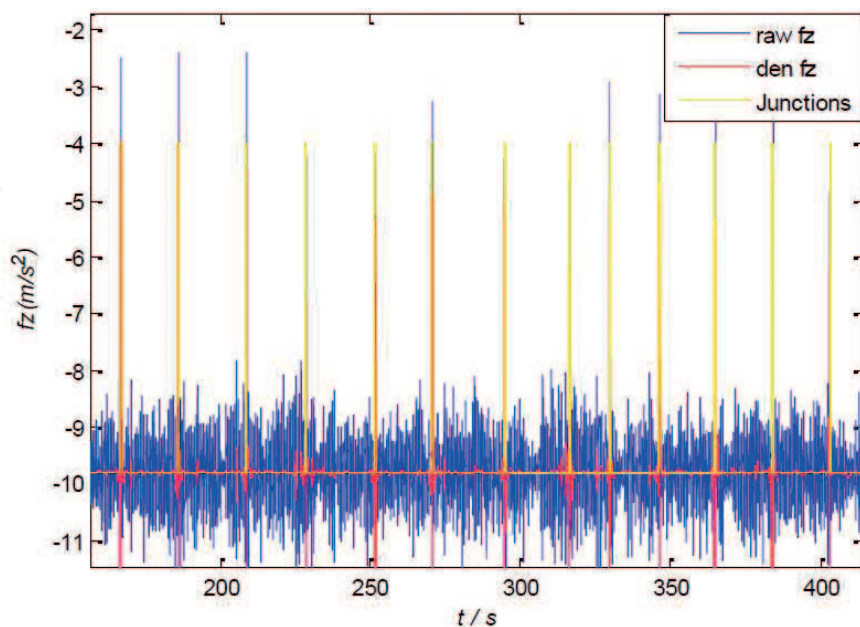


Figure 10. The PJ detection results by FOS.

signal-to-noise ratio of accelerometer measurement data could be improved greatly. In addition, the yellow curve in **Figure 10** is the PJ detection results; the spike intervals display that the Husky A200™ robot is passing a 90° corridor or a preset protrusion, while the rest of the intervals represents the robot going through the straight corridor segment.

5.3.2. EKF- and RTSS-estimated results

The EKF-estimated PIG navigation system result is shown in **Figure 11** by the blue trajectory. It only utilizes the forward velocity provided by the odometers and also the PIG NHCs updates to reduce the system error. The maximum position error of the blue trajectory is 18.93 m in the eighth landmark, and meanwhile, the corresponding mean error is 10.86 m. Meanwhile, the azimuth and pitch errors correction in each SPS of the PIG navigation system is provided by the PJ detection result. And the EKF/PJ-estimated PIG navigation system is shown in **Figure 11** with yellow trajectory. The maximum position error of yellow trajectory is 8.75 m in the eighth landmark, and the corresponding mean error is 4.96 m. So, the mean error of PIG navigation system improves 54.328% at all eight landmarks after adding the azimuth and pitch errors correction by EKF/PJ estimation. However, the position precision of EKF estimation technique on micro-inertial sensors still cannot fulfill the precision requirements of PIG navigation system when the azimuth and pitch errors correction are added in SPS. Fortunately, the RTSS offline estimation technology can be used to improve the position precision of the PIG navigation system once after the EKF estimated result.

In **Figure 12**, the blue curve denotes the trajectory of EKF- and RTSS-estimated PIG navigation system with 3D continuous velocity error and 3D coordinate correction at the starting point. The maximum position error of blue trajectory at the fifth landmark is 6.62 m, and the corresponding mean error is 3.73 m. In addition, the PJ-identified azimuth and pitch errors correction at the SPS is also utilized to improve the position precision of PIG navigation

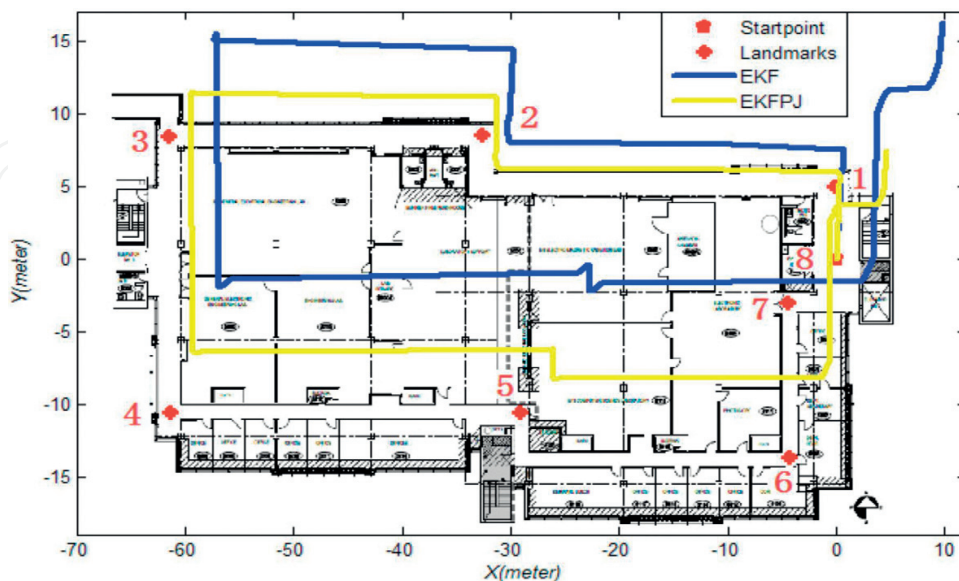


Figure 11. The trajectories of EKF-estimated PIG navigation system.

system. The yellow trajectory is the result of the EKF/PJ/RTSS-estimated PIG navigation system. The maximum position error of blue trajectory is 3.08 m at the fifth landmark, and the corresponding mean error is 1.70 m. Therefore, the mean error of PIG navigation system at the overall eight landmarks improves 54.42% after adding azimuth and pitch errors correction with EKF/RTSS estimation technology.

Subsequently, the statistic results of PIG navigation system errors at all eight landmarks that are optimized by EKF, EKF/PJ, EKF/RTSS, and EKF/PJ/RTSS are listed in **Table 1**. Specifically, the second column is position errors of PIG navigation system estimated by EKF when it is compared with the referenced eight landmarks. The position errors are increased with the PIG traveling distance from 1.96 m at first landmark to 18.93 m at last landmark. Then, the third

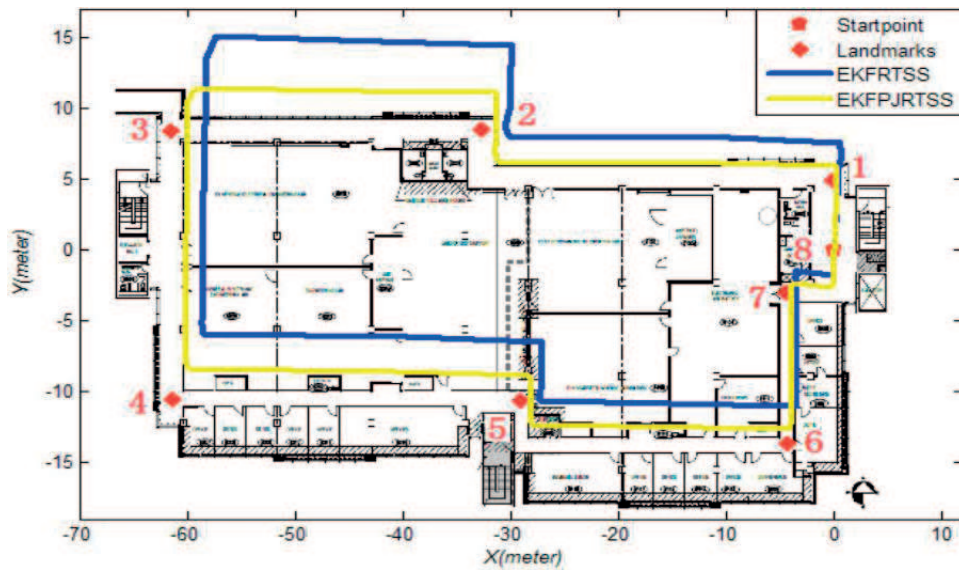


Figure 12. The trajectories of EKF/RTSS-estimated PIG navigation system.

Landmarks	EKF	EKF/PJ	EKF/RTSS	EKF/PJ/RTSS
1 (m)	1.96	0.76	1.98	1.01
2 (m)	5.77	2.53	2.77	1.28
3 (m)	8.06	3.81	4.14	1.75
4 (m)	10.03	4.74	5.73	2.76
5 (m)	11.39	5.08	6.62	3.08
6 (m)	14.53	6.59	6.24	2.78
7 (m)	16.19	7.44	2.37	0.93
8 (m)	18.93	8.75	0	0
Max (m)	18.93	8.75	6.62	3.08
Mean (m)	10.86	4.96	3.73	1.7

Table 1. The statistic result of PIG navigation system error.

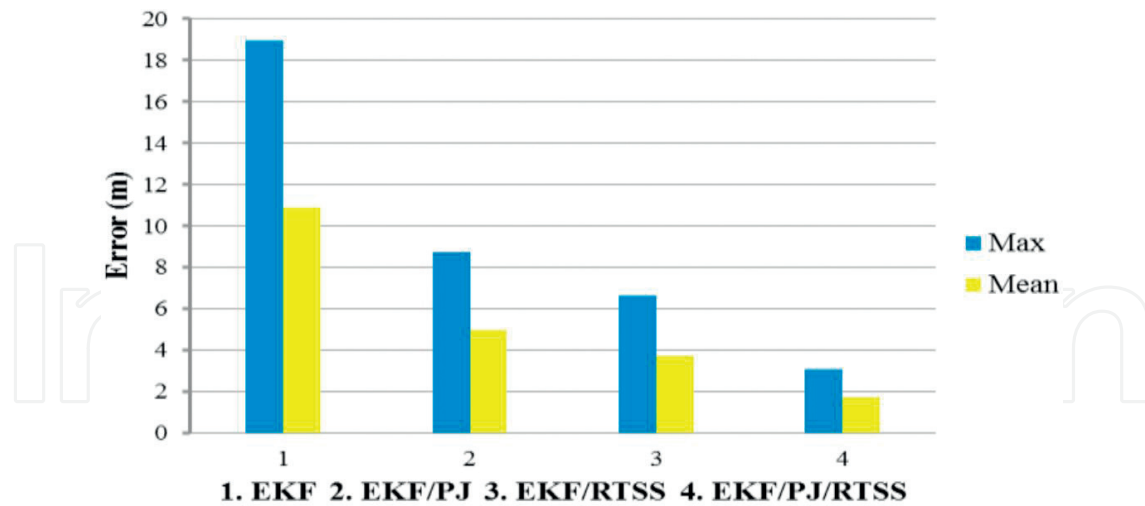


Figure 13. The errors of PIG navigation system by various optimization methods.

column is position errors of PIG navigation system that is estimated by EKF/PJ when it is compared with the referenced eight landmarks. The position errors are increased with the PIG traveling distance from 0.76 m at first landmark to 8.75 m at last landmark. In addition, the fourth and fifth columns of **Table 1** denote position errors of PIG navigation system when it is referenced to all eight landmarks that are estimated by EKF/RTSS and EKF/RTSS/PJ techniques. The maximum errors estimated by EKF/RTSS and EKF/RTSS/PJ are 6.62 and 3.08 m at the fifth landmark that has the longest distance from the start point or coordinate update point. This is mainly because of the inverse correction by RTSS, which reduces the position error of PIG navigation system when the trajectory is close to the coordinate update points. Therefore, both the maximum error and mean error are improved by the RTSS estimation technique.

More intuitively, both the maximum and mean errors of the PIG navigation system estimated by EKF, EKF/PJ, EKF/RTSS, and EKF/PJ/RTSS are shown by column chart in **Figure 13**. Both maximum and mean errors are improved greatly when adding the PJ detection result and the RTSS estimation technique.

6. Conclusions

This chapter presents a micro-inertial-aided high-precision positioning method for small-diameter PIG navigation, which is based on the micro-inertial/AGM/odometer/PJ PIG navigation system. Apart from the previous 3D continuous velocity updates from odometers and NHCs and the 3D sporadic coordinate updates from AGMs, the proposed micro-inertial/AGM/odometer/PJ-based PIG navigation system also adds continuous azimuth and pitch error correction in each SPS to reduce the divergent SINS-error-induced PIG navigation error. Furthermore, an indoor-Husky-robot-simulated PIG experiment is implemented to testify the performance of the PJ detection result on PIG navigation system, and the mean error of PIG navigation system improved 54.42% after adding azimuth and pitch errors correction by EKF/RTSS estimation technique.

Acknowledgements

This work was sponsored by the National Natural Science Foundation of China (61803118), the Science and Technology Research Program of Chongqing Municipal Education Commission (KJZD-K201804701), the Post Doc. Foundation of Heilongjiang Province (LBH-Z17053) and the Fundamental Research Funds for the Central Universities (HEUCFJ180402).

Author details

Lianwu Guan^{1*}, Xu Xu¹, Yanbin Gao¹, Fanming Liu¹, Hanxiao Rong¹, Meng Wang¹ and Aboelmagd Noureldin²

*Address all correspondence to: guanlianwu@hrbeu.edu.cn

1 College of Automation, Harbin Engineering University, Harbin, China

2 Department of Electrical and Computer Engineering, Queen's University, Kingston, Canada

References

- [1] Coramik M, Ege Y. Discontinuity inspection in pipelines: A comparison review[J]. *Measurement*. 2017;**111**:359-373. DOI: 10.1016/j.measurement.2017.07.058
- [2] Available from: <https://cepa.com/en/> [Accessed: 29-06-2016]
- [3] Ben Y, Yang J, Yin D, Li Q. System reset of strapdown INS for pipeline inspection gauge. *Ocean Engineering*. 2014;**88**:357-365. DOI: 10.1016/j.oceaneng.2014.07.004
- [4] Gloria NBS, Areiza MCL, Miranda IVJ, Rebello JMA. Development of a magnetic sensor for detection and sizing of internal pipeline corrosion defects. *NDT and E International*. 2009;**42**(8):669-677. DOI: 10.1016/j.ndteint.2009.06.009
- [5] Wenman T, Dim JC. Pipeline integrity management. In: *ICPTT 2011@Sustainable Solutions for Water, Sewer, Gas, and Oil Pipelines*. ASCE; 2012. pp. 1532-1540. DOI: 10.2118/161948-MS
- [6] Liu Z, Kleiner Y. State of the art review of the inspection technologies for condition assessment of water pipes. *Measurement*. 2013;**46**:1-15. DOI: 10.1016/j.measurement.2012.05.032
- [7] Gao Y, Guan L, Wang T. Optimal artificial fish swarm algorithm for the field calibration on marine navigation. *Measurement*. 2014;**50**:297-304. DOI: 10.1016/j.measurement.2014.01.003
- [8] Martell HE. Applications of strapdown inertial systems in curvature detection problems. *International Hepatology Communications*. 1991;**3**(95):147-147. DOI: 10.5072/PRISM/18281
- [9] Guan L, Gao Y, Osman A, et al. Analysis of rolling motion effect on SINS error modeling in PIG, IEEE/ION position, location and navigation symposium (PLANS). Savannah, GA: IEEE; 2016. pp. 681-686. DOI: 10.1109/PLANS.2016.7479761

- [10] Guan L, Gao Y, Osman A, et al. Pipeline junction detection from accelerometer measurement using fast orthogonal search, position, location and navigation symposium. IEEE. 2016;21-26. DOI: 10.1109/PLANS.2016.7479678
- [11] Sahli H, Moussa A, Noureldin A, et al. Small pipeline trajectory estimation using MEMS based IMU. In: Proceedings of the 27th International Technical Meeting of The Satellite Division of the Institute of Navigation (ION GNSS+ 2014); September 2014; Tampa, Florida. pp. 154-161
- [12] Kok M, Schön TB. Maximum likelihood calibration of a magnetometer using inertial sensors. IFAC Proceedings Volumes. 2014;47(3):92-97. DOI: 10.3182/20140824-6-ZA-1003.02025
- [13] Hanna PL. Strapdown inertial systems for pipeline navigation. In: Inertial Navigation Sensor Development, IEE Colloquium on IET. 2002. pp. 7/1-7/3
- [14] Noureldin A, Karamat TB, Georgy J. Fundamentals of Inertial Navigation, Satellite-based Positioning and their Integration. Springer Berlin Heidelberg; 2013. DOI: 10.1007/978-3-642-30466-8
- [15] Ernst HK. The rolling pig or how does a survey creep through a pipeline. Bulletin Geodesique. 1994;68(2):71-76. DOI: 10.1007/BF00819383
- [16] Korenberg MJ, Paarmann LD. Orthogonal approaches to time-series analysis and system identification. IEEE Signal Processing Magazine. 1991;8(3):29-43. DOI: 10.1109/79.127999
- [17] Chon KH. Accurate identification of periodic oscillations buried in white or colored noise using fast orthogonal search. IEEE Transaction on Biomedical Engineering. 2001;48(6):622-629. DOI: 10.1109/10.923780
- [18] Shen Z, Georgy J, Korenberg MJ, Noureldin A. Nonlinear modeling and identification of inertial errors with application to 2D vehicle navigation. In: Proceedings of the 22nd International Technical Meeting of The Satellite Division of the Institute of Navigation (ION GNSS 2009), International Journal of Navigation and Observation; New York, USA. 2009. pp. 593-599
- [19] Noureldin A, Armstrong J, El-Shafie A, et al. Accuracy enhancement of inertial sensors utilizing high resolution spectral analysis. Sensors. 2012;12(9):11638-11660. DOI: 10.3390/s120911638
- [20] Shen Z, Georgy J, Korenberg M, Noureldin A. FOS-based modeling of reduced inertial sensor system errors for 2D vehicular navigation. Electronics Letters. 2010;46:298-299. DOI: 10.1049/el.2010.2507
- [21] Chowdhury MS, Abdelhafez MF. Pipeline inspection gauge position estimation using inertial measurement unit, odometer, and a set of reference stations. Sensors and Actuators B: Chemical. 2016;2(3):234-243. DOI: 10.1115/1.4030945
- [22] Guan L, Cong X, Sun Y, et al. Enhanced MEMS SINS aided pipeline surveying system by pipeline junction detection in small diameter pipeline[J]. IFAC-PapersOnLine. 2017; 50(1):3560-3565. DOI: 10.1016/j.ifacol.2017.08.962